

Article

# Enhanced Microwave Absorption and Surface Wave Attenuation Properties of $\text{Co}_{0.5}\text{Ni}_{0.5}\text{Fe}_2\text{O}_4$ Fibers/Reduced Graphene Oxide Composites

Yinrui Li, Dongmeng Li, Jing Yang, Hui Luo \*, Fu Chen, Xian Wang and Rongzhou Gong

School of Optical and Electronic Information, Huazhong University of Science and Technology, Wuhan 430074, China; li\_yinrui@163.com (Y.L.); eileen\_lee@hust.edu.cn (D.L.); quark@hust.edu.cn (J.Y.); zs101141@163.com (F.C.); wangx@hust.edu.cn (X.W.); rzhgong@hust.edu.cn (R.G.)

\* Correspondence: luohui0112@163.com; Tel.: +86-131-6337-2989

Received: 7 February 2018; Accepted: 26 March 2018; Published: 28 March 2018



**Abstract:**  $\text{Co}_{0.5}\text{Ni}_{0.5}\text{Fe}_2\text{O}_4$  fibers with a diameter of about 270 nm and a length of about 10  $\mu\text{m}$  were synthesized by a microemulsion-mediated solvothermal method with subsequent heat treatment. The  $\text{Co}_{0.5}\text{Ni}_{0.5}\text{Fe}_2\text{O}_4$  fibers/reduced graphene oxide (RGO) composite was prepared by a facile in-situ chemical reduction method. The crystalline structures and morphologies were investigated based on X-ray diffraction patterns and scanning electron microscopy. Magnetization measurements were carried out using a vibrating sample magnetometer at room temperature.  $\text{Co}_{0.5}\text{Ni}_{0.5}\text{Fe}_2\text{O}_4$  fibers/RGO composites achieve both a wider and stronger absorption and an adjustable surface wave attenuation compared with  $\text{Co}_{0.5}\text{Ni}_{0.5}\text{Fe}_2\text{O}_4$  fibers, indicating the potential for application as advanced microwave absorbers.

**Keywords:**  $\text{Co}_{0.5}\text{Ni}_{0.5}\text{Fe}_2\text{O}_4$  fiber; RGO; microwave absorption properties; surface wave attenuation

## 1. Introduction

Microwave absorbing materials with the properties of thinness, lightweight, broadband and strong absorption have received increasing attention due to their pragmatic and effective functions for reducing electromagnetic interference (EMI) pollution and defense stealth technology. The specular reflection, cavity or ducting scattering, and angular scattering as the major potential scattering source of stealth objects can be sufficiently suppressed by shaping of the objects and the use of radar absorbing materials (RAM) [1–7]. As far as we know, there is almost no work discussing reflection loss and surface wave attenuation together [8]. Therefore, there is an urgent need to prepare a new generation of absorbers to realize low reflection loss and strong surface wave attenuation together.

In recent years, extensive attention has been aroused regarding magnetic shape-controlled materials due to their technological applications such as medical diagnostics, high-density magnetic recording media, optical and mechanic devices, catalysts, advanced magnetic materials, and Ferro-fluids [9–14]. It is also reported that peculiar morphologies of the materials are also beneficial to their microwave absorption properties [15,16]. Besides the typical ferromagnetic materials such as iron, cobalt and nickel, spinel type ferrites also have been considered as one of the most promising microwave absorbing materials due to their low cost and high abundance [17–20]. But the high density and low surface area limit their applications as absorbers [21]. Compared with traditional ferrite materials, carbon-based composite materials have advantages, such as low density and high surface area, which can promote the microwave absorption ability [22–28]. Reduced graphene oxide with internal residual defects and groups not only improves the impedance match characteristic but also introduces polarization relaxation and electronic dipole relaxation, which are beneficial for microwave

penetration and absorption [29]. The microwave absorption properties of  $\text{Co}_{0.5}\text{Ni}_{0.5}\text{Fe}_2\text{O}_4$  fibers and reduced graphene oxide composites have not been reported.

In this study, we report the microwave absorption and surface wave attenuation properties of  $\text{Co}_{0.5}\text{Ni}_{0.5}\text{Fe}_2\text{O}_4$  fibers/RGO composites. The results show that  $\text{Co}_{0.5}\text{Ni}_{0.5}\text{Fe}_2\text{O}_4$  fibers and the reduced graphene oxide worked synergistically as the magnetic loss absorber and dielectric loss absorber, respectively, and enhanced the microwave absorption properties. This work evaluates reflection loss and surface wave attenuation of one absorber simultaneously. More interestingly,  $\text{Co}_{0.5}\text{Ni}_{0.5}\text{Fe}_2\text{O}_4$  fibers/RGO composites show great surface wave attenuation properties with adjustable attenuation frequency band, thus making it an advanced absorber.

## 2. Experimental Section

In a typical preparation, graphene oxide (GO) was prepared from natural graphite by using a modified Hummers method [30]. The precursor of  $\text{Co}_{0.5}\text{Ni}_{0.5}\text{Fe}_2\text{O}_4$  fibers were synthesized in a microemulsion system. In the typical procedure, CTAB (1.6 g) was dissolved in a mixture of 120 mL cyclohexane and 4 mL n-pentanol and stirred for 30 min. Then, a mixed aqueous solution (6 mL) containing  $\text{H}_2\text{C}_2\text{O}_4 \cdot \text{H}_2\text{O}$  (1.21 g) was added to the mixture and stirred for another 1 h. Finally, 2 mL aqueous solution containing  $\text{CoSO}_4 \cdot 7\text{H}_2\text{O}$  (0.028 g),  $\text{NiSO}_4 \cdot 6\text{H}_2\text{O}$  (0.026 g) and  $\text{FeSO}_4 \cdot 7\text{H}_2\text{O}$  (0.111 g) was added to the microemulsion drop by drop. After substantial stirring, the microemulsion was transferred into a stainless Teflon-lined autoclave and heat at 80 °C for 6 h, then cooled to room temperature naturally. The solid product was washed with propanone and ethanol several times and then dried. The  $\text{Co}_{0.5}\text{Ni}_{0.5}\text{Fe}_2\text{O}_4$  fibers were obtained by heat treatment of the precursors of  $\text{Co}_{0.5}\text{Ni}_{0.5}\text{Fe}_2\text{O}_4$  fibers at 700 °C for 3 h. The  $\text{Co}_{0.5}\text{Ni}_{0.5}\text{Fe}_2\text{O}_4$  fibers/reduced graphene oxide composite was synthesized in the solution by stirring suspension of  $\text{Co}_{0.5}\text{Ni}_{0.5}\text{Fe}_2\text{O}_4$  fibers (100 mg) and graphene oxide (GO) powders (100 mg) in a mixture of 100 mL water and 5 mL aqueous hydrazine ( $\text{N}_2\text{H}_4 \cdot \text{H}_2\text{O}$ , 80% concentration) for 2 h at 90 °C. After being centrifuged and dried, the  $\text{Co}_{0.5}\text{Ni}_{0.5}\text{Fe}_2\text{O}_4$  fiber/RGO composites were obtained.

The crystalline structures of the as-synthesized samples were studied by X-ray powder diffraction (XRD, XRD-7000, SHIMADZU, Kyoto, Japan) using  $\text{Cu K}\alpha$  radiation ( $\lambda = 0.154187 \text{ \AA}$ ), with the scanning rate of  $0.02^\circ \text{ S}^{-1}$  in the  $2\theta$  range of  $5^\circ$ – $70^\circ$ . Scanning Electron Microscopy (SEM, Nova NanoSEM 450, FEI, Shanghai, China) was used to characterize the morphology of the samples. Magnetic properties were studied using a Lakeshore 7404 vibrating sample magnetometer with an applied magnetic field of  $\pm 15 \text{ kOe}$ . Toroidal-shaped samples (inner diameter 3.04 mm, outer diameter 7 mm) with the weight ratio of samples to paraffin 3:7 were prepared to fit well the coaxial sample holder for microwave measurements. The complex permeability and permittivity of the test samples were examined over the frequency range of 300 MHz–18 GHz by reflection and transmission method carried out by an Agilent E5071C vector network analyzer.

## 3. Results and Discussion

Figure 1 shows the typical X-ray diffraction (XRD) patterns of GO,  $\text{Co}_{0.5}\text{Ni}_{0.5}\text{Fe}_2\text{O}_4$  fibers and  $\text{Co}_{0.5}\text{Ni}_{0.5}\text{Fe}_2\text{O}_4$  fibers/RGO composites. Figure 1a shows the XRD pattern of GO. All the main peak values in the pattern in Figure 1b could be an index of the cubic crystalline phase of  $\text{NiFe}_2\text{O}_4$  (JCPDS card 03-0875) or  $\text{CoFe}_2\text{O}_4$  (JCPDS card 01-1121) with little deviation. The deviation is mainly caused by the (511) peak value  $57.40^\circ$ , of which the  $\text{NiFe}_2\text{O}_4$  is  $57.56^\circ$ ,  $\text{CoFe}_2\text{O}_4$  is  $57.17^\circ$ . This is mainly due to the variety of the lattice constants. As the lattice constants increase, the diffraction peaks shift left [31,32]. The last diffraction pattern in Figure 1c shows the  $\text{Co}_{0.5}\text{Ni}_{0.5}\text{Fe}_2\text{O}_4$  fibers/RGO composites. There is no diffraction peak around  $2\theta = 26^\circ$  in the  $\text{Co}_{0.5}\text{Ni}_{0.5}\text{Fe}_2\text{O}_4$  fibers/RGO composites, indicating that  $\text{Co}_{0.5}\text{Ni}_{0.5}\text{Fe}_2\text{O}_4$  fibers are efficiently assembled on the surface of RGO, suppressing the stacking of graphene layers and destroying the (002) interplanar periodic structure [33–35].

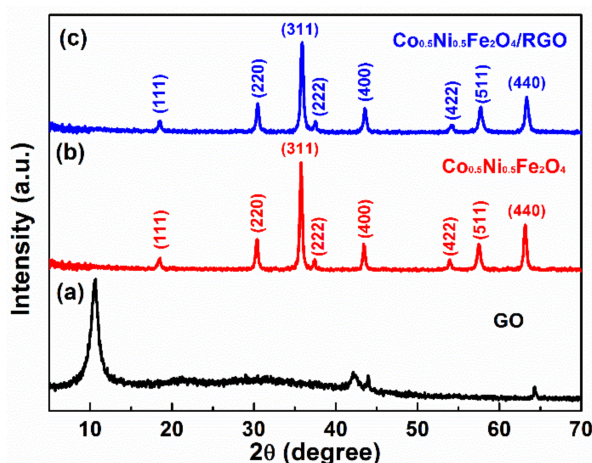


**Figure 1.** XRD patterns of the samples: (a) GO; (b)  $\text{Co}_{0.5}\text{Ni}_{0.5}\text{Fe}_2\text{O}_4$  fibers; (c)  $\text{Co}_{0.5}\text{Ni}_{0.5}\text{Fe}_2\text{O}_4$  fibers/RGO composites.

The as-prepared Co/Ni/Fe composites oxalate fibers have a mono-disperse and uniform fiber-like morphology as shown in Figure 2a. Figure 2b illustrates the precursor fibers have an average diameter of 600 nm and length of about 10  $\mu\text{m}$ . From the typical SEM image (Figure 2c), the morphology of the  $\text{Co}_{0.5}\text{Ni}_{0.5}\text{Fe}_2\text{O}_4$  fibers shows little change after calcination. The diameter of the  $\text{Co}_{0.5}\text{Ni}_{0.5}\text{Fe}_2\text{O}_4$  fibers decreases to about 200 nm with little change in length, and the surface of the fibers become a little rough, as shown in Figure 2d. The  $\text{Co}_{0.5}\text{Ni}_{0.5}\text{Fe}_2\text{O}_4$  fiber precursor is initially amorphous, but upon heat treatment, the  $\text{Co}_{0.5}\text{Ni}_{0.5}\text{Fe}_2\text{O}_4$  fibers nucleate internally and crystalline through not only “oriented attachment” but also directional coalescence, thus leading to the rough surface of the  $\text{Co}_{0.5}\text{Ni}_{0.5}\text{Fe}_2\text{O}_4$  fibers [36,37]. Figure 2e shows the prefabricated GO with layered structure. The  $\text{Co}_{0.5}\text{Ni}_{0.5}\text{Fe}_2\text{O}_4$  fibers are dispersed homogeneously and embedded inside as well as on the surface of the RGO, and the composites form large stratiform particles, as shown in Figure 2f.

The magnetic hysteresis curves for  $\text{Co}_{0.5}\text{Ni}_{0.5}\text{Fe}_2\text{O}_4$  fibers and  $\text{Co}_{0.5}\text{Ni}_{0.5}\text{Fe}_2\text{O}_4$  fibers/RGO composites were measured at room temperature, as shown in Figure 3. The saturation magnetization ( $M_s$ ) of  $\text{Co}_{0.5}\text{Ni}_{0.5}\text{Fe}_2\text{O}_4$  fibers and  $\text{Co}_{0.5}\text{Ni}_{0.5}\text{Fe}_2\text{O}_4$  fibers/RGO composites are 38.17 emu/g and 24.39 emu/g, respectively. The measured saturation magnetizations of  $\text{Co}_{0.5}\text{Ni}_{0.5}\text{Fe}_2\text{O}_4$  fibers/RGO composites are lower than those of  $\text{Co}_{0.5}\text{Ni}_{0.5}\text{Fe}_2\text{O}_4$  fibers because the RGO is diamagnetic at room temperature [29]. The coercivity of the  $\text{Co}_{0.5}\text{Ni}_{0.5}\text{Fe}_2\text{O}_4$  fibers and  $\text{Co}_{0.5}\text{Ni}_{0.5}\text{Fe}_2\text{O}_4$  fibers/RGO is almost the same.

The microwave absorbing properties of the materials are dominated by the magnetic and dielectric losses [17]. Figure 4 shows the measured complex permittivity and complex permeability in the frequency range of 0.3–18 GHz. Generally speaking, the real parts of complex permittivity and permeability symbolize the storage ability of electromagnetic energy, and the imaginary parts represent the electromagnetic energy loss ability [38]. According to the free electron theory,  $\epsilon'' \approx 1/2\pi\rho f\epsilon_0$ , where  $\rho$ ,  $f$  and  $\epsilon_0$  are the resistivity, the frequency and the dielectric constant of free space, respectively. It is found that both the real and imaginary parts of complex permittivity of the  $\text{Co}_{0.5}\text{Ni}_{0.5}\text{Fe}_2\text{O}_4$  fibers/RGO are obviously higher than  $\text{Co}_{0.5}\text{Ni}_{0.5}\text{Fe}_2\text{O}_4$  fibers because RGO possesses high conductive properties. The polarization loss can be divided into dipolar orientation polarization and interfacial polarization at microwave frequency [39]. The difference in dielectric constants and electrical conductivities among the paraffin, RGO and  $\text{Co}_{0.5}\text{Ni}_{0.5}\text{Fe}_2\text{O}_4$  fibers is responsible for the generation of interfacial polarization. For all samples, the variation of both the real and imaginary parts of the complex permeability is small, indicating a certain amount of magnetic loss contributions. Apart from dielectric loss and magnetic loss, another important concept relating to microwave absorption is the impedance match characteristic: too high permittivity of absorber is harmful to the impedance match and results in strong reflection and weak absorption [40].

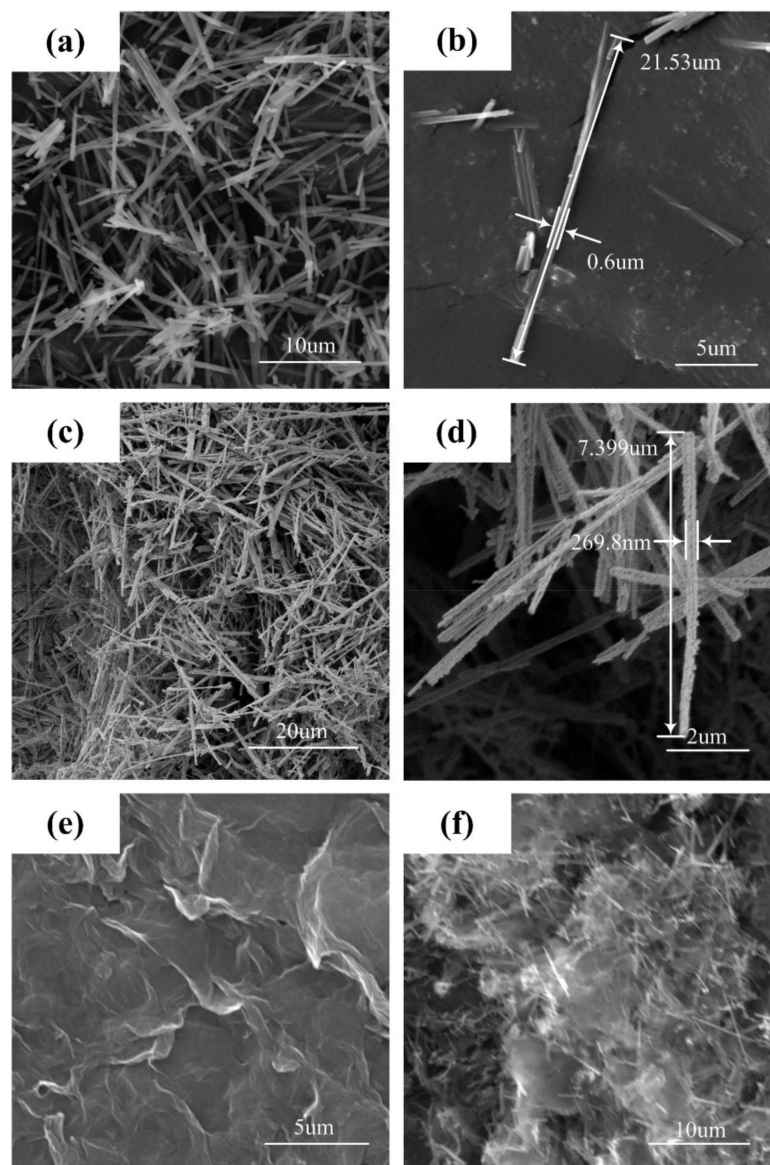


**Figure 2.** SEM images of the as-prepared powders: (a,b) Co/Ni/Fe composite oxalate fibers; (c,d)  $\text{Co}_{0.5}\text{Ni}_{0.5}\text{Fe}_2\text{O}_4$  fibers; (e) GO; (f)  $\text{Co}_{0.5}\text{Ni}_{0.5}\text{Fe}_2\text{O}_4$  fibers/RGO composites.

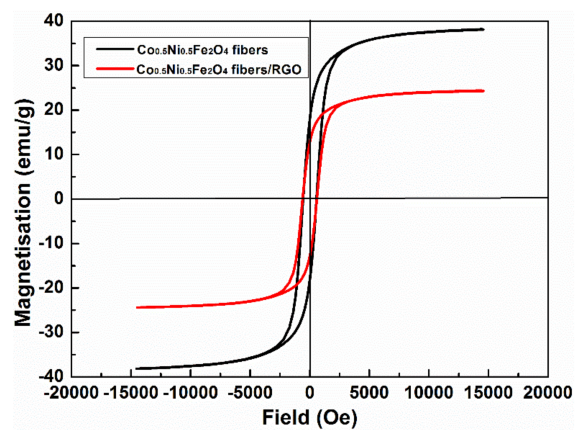


**Figure 3.** Magnetic hysteresis curves for  $\text{Co}_{0.5}\text{Ni}_{0.5}\text{Fe}_2\text{O}_4$  fibers and  $\text{Co}_{0.5}\text{Ni}_{0.5}\text{Fe}_2\text{O}_4$  fibers/RGO composites measured at room temperature.

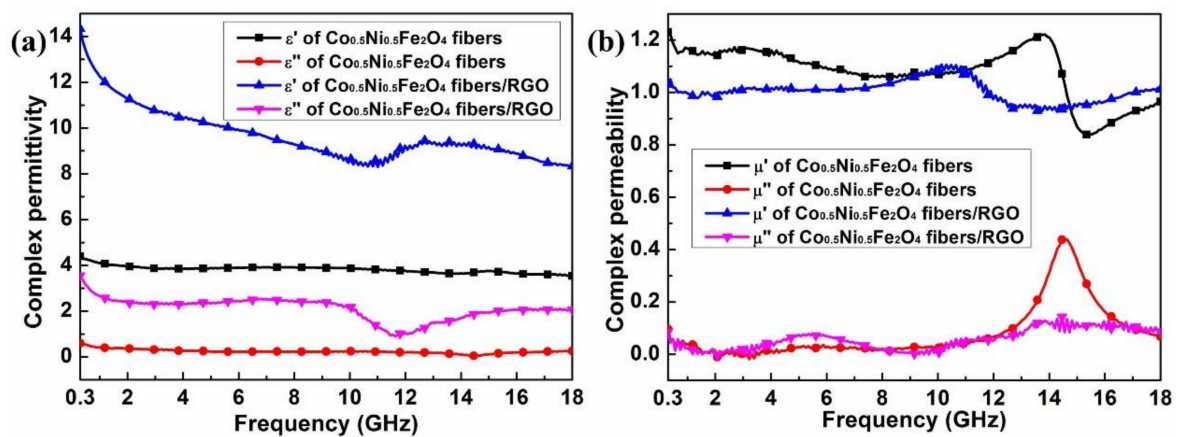


**Figure 4.** Frequency dependence of the relative complex electromagnetic parameters spectra: (a) Complex permittivity; (b) Complex permeability.

To evaluate the electromagnetic absorption performance of the samples, the reflection loss (RL) values were calculated based on the experimental data of the complex permittivity and permeability, and a single layer of the composite sample was assumed to be attached on a metal plate. The reflection loss RL (dB) is calculated by the following equations: [41,42]

$$RL = 20 \log |(Z_{in} - Z_0) / (Z_{in} + Z_0)| \quad (1)$$

$$Z_{in} = Z_0 \sqrt{(\mu_r / \epsilon_r) \tanh[j(2\pi f d / c) \sqrt{\mu_r \epsilon_r}]} \quad (2)$$

where  $Z_0$  is the impedance of free space,  $Z_{in}$  is the input impedance of the absorber,  $f$  is the frequency of the electromagnetic waves,  $c$  is the velocity of electromagnetic waves in free space,  $\mu_r$  and  $\epsilon_r$  are, respectively, the relative complex permeability and permittivity, and  $d$  is the thickness of the absorber.

The reflection loss (RL) of Co<sub>0.5</sub>Ni<sub>0.5</sub>Fe<sub>2</sub>O<sub>4</sub> fibers and Co<sub>0.5</sub>Ni<sub>0.5</sub>Fe<sub>2</sub>O<sub>4</sub> fibers/RGO with different thickness is shown in Figure 5. The thickness of the sample is one of the crucial parameters which affects the intensity and the position of the frequency at the reflection loss minimum [21]. This phenomenon has been successfully explained by the quarter-wavelength cancellation model in absorbers [43]. The maximum reflection loss reaches  $-13.1$  dB at 14.8 GHz and the absorption frequency range under  $-10$  dB (90% of EM wave absorption) is from 14.4 to 15.4 GHz for the Co<sub>0.5</sub>Ni<sub>0.5</sub>Fe<sub>2</sub>O<sub>4</sub> fibers containing samples with a thickness of 2.5 mm. With the variety of the thickness, the reflection loss under  $-5$  dB can be only tuned from 13.6 to 16.7 GHz. As shown in Figure 5b, the reflection loss of the sample containing Co<sub>0.5</sub>Ni<sub>0.5</sub>Fe<sub>2</sub>O<sub>4</sub> fibers/RGO less than  $-10$  dB was obtained in the 1.9 GHz (from 16.1 to 18 GHz) with the thickness of 1.5 mm. It is worth noting that the sample with a thickness of 2.0 mm shows a minimum reflection loss value of  $-14.7$  dB at 12.9 GHz. The minimum reflection loss peak moves drastically towards the lower frequency region with increasing thickness of the sample. With the variety of thickness, the effective absorption band width ( $RL \leq -10$  dB) can be tuned from 7.5 to 18 GHz, indicating adjustable microwave absorption properties.

Apart from dielectric loss and magnetic loss, impedance matching characteristic is another important parameter for microwave absorption and is calculated by the following equation: [44]

$$|Z_{in} / Z_0| = |\mu_r / \epsilon_r|^{1/2} |\tanh[j(2\pi f d / c) \sqrt{\mu_r \epsilon_r}]| \quad (3)$$

The frequency dependence of  $Z = |Z_{in} / Z_0|$  for the Co<sub>0.5</sub>Ni<sub>0.5</sub>Fe<sub>2</sub>O<sub>4</sub> fibers and Co<sub>0.5</sub>Ni<sub>0.5</sub>Fe<sub>2</sub>O<sub>4</sub> fibers/RGO composites was obtained, as presented in Figure 6. It is illustrated in Figure 6b that the minimum RL of Co<sub>0.5</sub>Ni<sub>0.5</sub>Fe<sub>2</sub>O<sub>4</sub> fibers/RGO composites can be obtained and the corresponding  $Z$  is most close to 1 when the matching frequency is 12.9 GHz and the matching thickness is 2.0 mm.

On the contrary, the impedance matching characteristic of  $\text{Co}_{0.5}\text{Ni}_{0.5}\text{Fe}_2\text{O}_4$  fibers is poor compared with  $\text{Co}_{0.5}\text{Ni}_{0.5}\text{Fe}_2\text{O}_4$  fibers/RGO composites, as shown in Figure 6a.

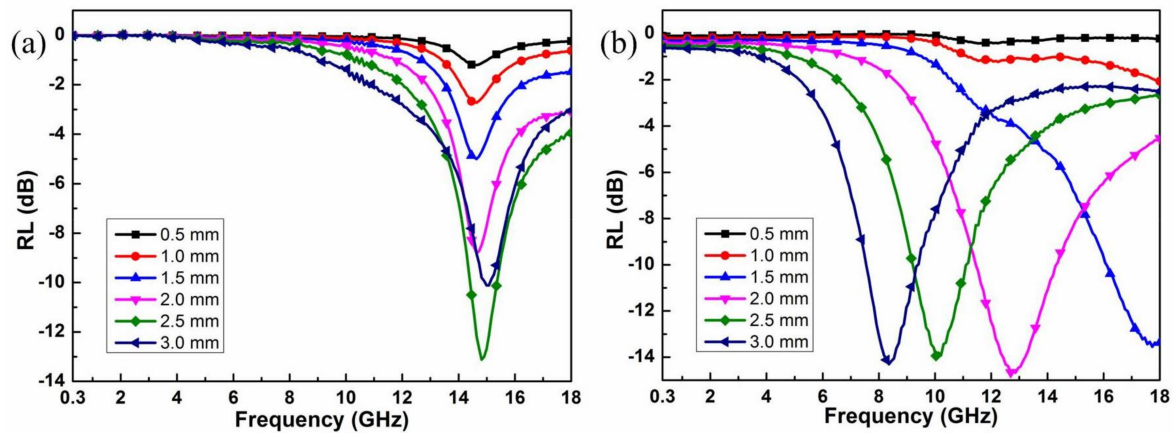


Figure 5. The calculated reflection loss: (a)  $\text{Co}_{0.5}\text{Ni}_{0.5}\text{Fe}_2\text{O}_4$  fibers; (b)  $\text{Co}_{0.5}\text{Ni}_{0.5}\text{Fe}_2\text{O}_4$  fibers/RGO.

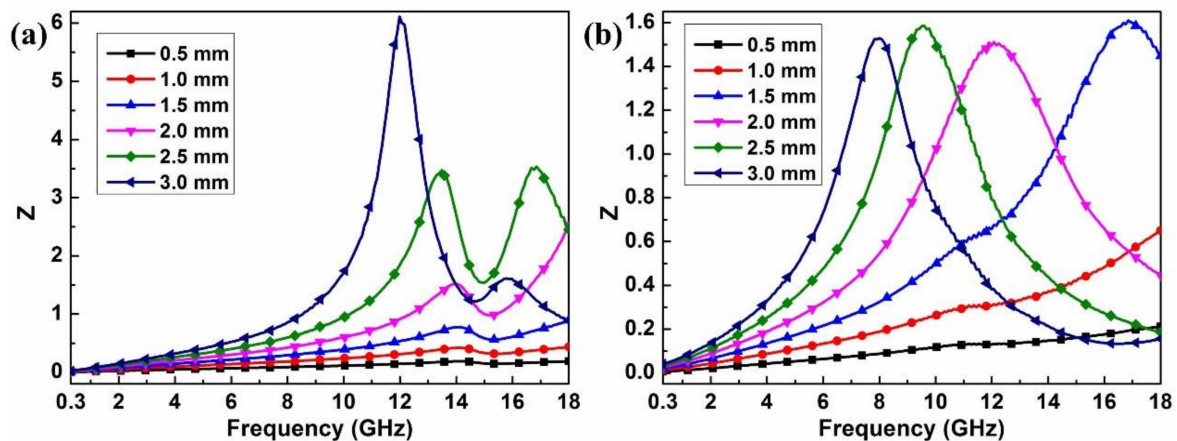


Figure 6. The modulus of normalized input impedance ( $|Z_{in}/Z_0|$ ): (a)  $\text{Co}_{0.5}\text{Ni}_{0.5}\text{Fe}_2\text{O}_4$  fibers; (b)  $\text{Co}_{0.5}\text{Ni}_{0.5}\text{Fe}_2\text{O}_4$  fibers/RGO.

The enhanced absorption properties of  $\text{Co}_{0.5}\text{Ni}_{0.5}\text{Fe}_2\text{O}_4$  fibers/RGO composites can be explained by the following facts. First, the multi-interfaces and triple junctions ( $\text{RGO}@ \text{Co}_{0.5}\text{Ni}_{0.5}\text{Fe}_2\text{O}_4$ ,  $\text{RGO}@ \text{paraffin}$ ,  $\text{Co}_{0.5}\text{Ni}_{0.5}\text{Fe}_2\text{O}_4@ \text{paraffin}$ ) are advantageous for electromagnetic attenuation due to the existing interfacial polarization [45]. Second, RGO provides a large receptive surface for individual dispersion of  $\text{Co}_{0.5}\text{Ni}_{0.5}\text{Fe}_2\text{O}_4$  fibers and acts as an excellent substrate for the absorption of microwave, providing more active sites for reflection and scattering of electromagnetic waves, which makes both dielectric loss and magnetic loss work synergistically [46]. Third, the defects in the RGO can act as polarization and scattering centers introducing dielectric loss. Fourth, the impedance matching changed after the RGO was introduced, which can be seen in Figure 6.

Evaluating reflection loss and surface wave attenuation together is a wise choice, because non-specular reflection resulting from surface wave also contributes substantially to the radar cross section (RCS). A single layer of the composite sample is assumed to be attached to an infinite metal plate, and the surface wave attenuation constants  $\beta''$  were calculated based on the classic dispersion equations: [47]

$$D(k_0, \beta) \equiv \sqrt{k_0^2 \epsilon_r \mu_r - \beta^2} \tan \left( d \sqrt{k_0^2 \epsilon_r \mu_r - \beta^2} \right) + j \epsilon_r \sqrt{k_0^2 - \beta^2} = 0 \quad (4)$$

where  $k_0 = \omega\sqrt{\epsilon_0\mu_0}$  is the wave number of the free space,  $d$  is the thickness of the absorber. The quantity  $\beta$  is the longitudinal wave number, or the propagation constant, and  $\beta''$ , the imaginary part of  $\beta$ , is the surface wave attenuation constant.

The surface wave attenuation constant ( $\beta''$ ) of  $\text{Co}_{0.5}\text{Ni}_{0.5}\text{Fe}_2\text{O}_4$  fibers and  $\text{Co}_{0.5}\text{Ni}_{0.5}\text{Fe}_2\text{O}_4$  fibers/RGO with different thickness is shown in Figure 7. All the samples with the thickness of 0.5 mm show weak attenuation properties. There are nearly no attenuation abilities in the frequency range of 0.3–8 GHz for the  $\text{Co}_{0.5}\text{Ni}_{0.5}\text{Fe}_2\text{O}_4$  fibers samples with different thickness, as shown in Figure 7a. The attenuation reaches a certain intensity in the frequency range of 12–18 GHz which can attenuate surface waves sufficiently. But after the attenuation constants reach the maximum value at about 14.3 GHz, then decrease sharply. As for the  $\text{Co}_{0.5}\text{Ni}_{0.5}\text{Fe}_2\text{O}_4$  fibers/RGO samples, the attenuation constants reach their maximum value and then decrease with a further increase in frequency. The attenuation constants reach zero values and then become negative. Negative values of  $\beta''$  result from non-physical solutions of the dispersion equation. They imply the amplification of the field, rather than energy absorption, and must be ignored. Physically, these negative values mean that surface waves cannot be excited and thus no propagation occurs along the layers. The frequency at which the quantity  $\beta''$  vanishes can be considered as the upper cutoff frequency [48,49]. As the thickness of the sample increases, the upper cutoff frequency moves to the lower frequency, as shown in Figure 7b. Compared with  $\text{Co}_{0.5}\text{Ni}_{0.5}\text{Fe}_2\text{O}_4$  fibers, the attenuation frequency band of the sample  $\text{Co}_{0.5}\text{Ni}_{0.5}\text{Fe}_2\text{O}_4$  fibers/RGO can be adjusted and maintain a high attenuation constant value, showing good surface wave attenuation properties.

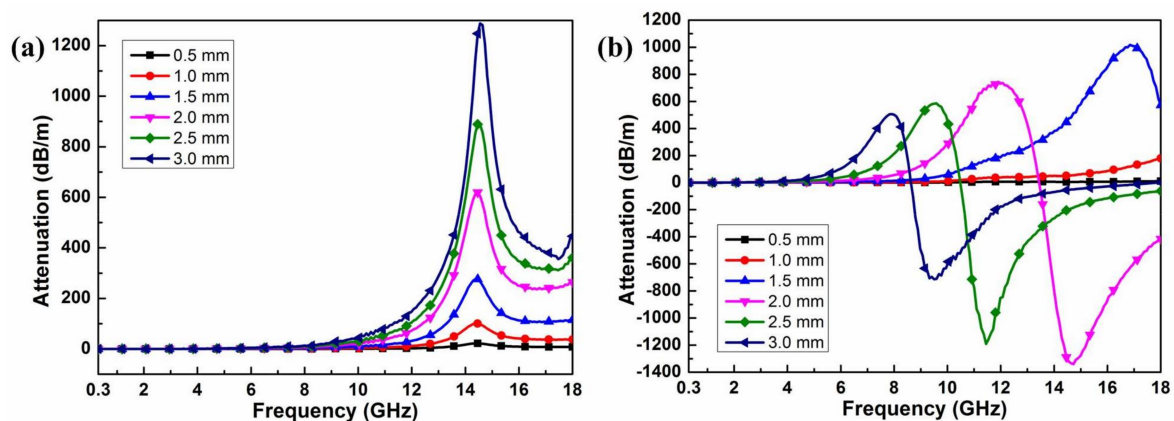


**Figure 7.** The calculated surface wave attenuation constants: (a)  $\text{Co}_{0.5}\text{Ni}_{0.5}\text{Fe}_2\text{O}_4$  fibers; (b)  $\text{Co}_{0.5}\text{Ni}_{0.5}\text{Fe}_2\text{O}_4$  fibers/RGO.

#### 4. Conclusions

In summary,  $\text{Co}_{0.5}\text{Ni}_{0.5}\text{Fe}_2\text{O}_4$  fibers have been prepared by a microemulsion-mediated solvothermal method and heat treatment. The composites of  $\text{Co}_{0.5}\text{Ni}_{0.5}\text{Fe}_2\text{O}_4$  fiber/RGO were prepared by the in-situ chemical reduction method. The  $\text{Co}_{0.5}\text{Ni}_{0.5}\text{Fe}_2\text{O}_4$  fibers retained the original fiber-like morphology throughout the whole calcination procedure. The microwave absorption properties of  $\text{Co}_{0.5}\text{Ni}_{0.5}\text{Fe}_2\text{O}_4$  fibers/RGO composites are higher compared with the  $\text{Co}_{0.5}\text{Ni}_{0.5}\text{Fe}_2\text{O}_4$  fiber. The enhanced microwave absorption properties are due to the magnetic loss absorber Co-Ni ferrite fibers and dielectric loss absorber RGO working synergistically. The  $\text{Co}_{0.5}\text{Ni}_{0.5}\text{Fe}_2\text{O}_4$  fiber/RGO composites show great surface wave attenuation properties with adjustable frequency band. This work provides a facile method for preparation of  $\text{Co}_{0.5}\text{Ni}_{0.5}\text{Fe}_2\text{O}_4$  fiber/RGO composites with great potential application as an advanced absorber for microwave absorption, especially in situations where surface wave attenuation is highly demanded.

**Acknowledgments:** This work was supported by the Natural Science Foundation of China (Grant No. 61701185) and the China Postdoctoral Science Foundation funded project (Grant No. 2017M622444).

**Author Contributions:** Yinrui Li and Hui Luo designed the experiments and wrote the paper; Dongmeng Li performed the experiments and completed the corresponding test; Jing Yang completed the corresponding calculations and analyzed the data; Fu Chen provided theoretical direction; Xian Wang and Rongzhou Gong modified the article and are tutors.

**Conflicts of Interest:** The authors declare no conflict of interest.

## References

1. Lim, W.G.; Yu, J.W. Scattering by a dielectric-loaded conducting wedge with concaved edge: TE case. *Prog. Electromagn. Res.* **2009**, *89*, 85–100. [[CrossRef](#)]
2. Terracher, F.; Berginc, G. Scattering by doubly periodic gaps and cracks. *J. Electromagn. Waves Appl.* **2000**, *14*, 1143–1158. [[CrossRef](#)]
3. Ivrišsimtzis, L.P.; Marhefka, R.J. Edge-wave diffraction for flat-plate structures. *IEE Proc. Microw. Antennas Propag.* **1994**, *141*, 30–36. [[CrossRef](#)]
4. Hu, X.J.; Ge, D.B. Study on conformal FDTD for electromagnetic scattering by targets with thin coating. *Prog. Electromagn. Res.* **2008**, *79*, 305–319. [[CrossRef](#)]
5. Oraizi, H.; Abdolali, A. Ultra wide band RCS optimization of multilayered cylindrical structures for arbitrarily polarized incident plane waves. *Prog. Electromagn. Res.* **2008**, *78*, 129–157. [[CrossRef](#)]
6. Yan, W.Z.; Du, Y.; Wu, H.; Liu, D.; Wu, B.I. EM scattering from a long dielectric circular cylinder. *Prog. Electromagn. Res.* **2008**, *85*, 39–67. [[CrossRef](#)]
7. Ding, D.Z.; Chen, R.S. Electromagnetic scattering by conducting bor coated with chiral media above a lossy half-space. *Prog. Electromagn. Res.* **2010**, *104*, 385–401. [[CrossRef](#)]
8. Chen, H.Y.; Lu, L.J.; Guo, D.J.; Lu, H.P.; Zhou, P.H.; Xie, J.L.; Deng, L.J. Relationships between Surface Wave Attenuation and the Reflection Properties of Thin Surface Wave Absorbing Layer. In Proceedings of the PIERS 2014, Guangzhou, China, 25–28 August 2014; pp. 1146–1150.
9. Caruso, F.; Spasova, M.; Susha, A.; Giersig, M.; Caruso, R.A. Magnetic nanocomposite particles and hollow spheres constructed by a sequential layering approach. *Chem. Mater.* **2001**, *13*, 109–116. [[CrossRef](#)]
10. Hyeon, T.; Lee, S.S.; Park, J.; Chung, Y.; Na, H.B. Synthesis of highly crystalline and monodisperse maghemite nanocrystallites without a size-selection process. *J. Am. Chem. Soc.* **2001**, *123*, 12798–12801. [[CrossRef](#)] [[PubMed](#)]
11. Xiong, Y.; Xie, Y.; Chen, S.; Li, Z. Fabrication of Self-Supported Patterns of Aligned  $\beta$ -FeOOH Nanowires by a Low-Temperature Solution Reaction. *Chem. A Eur. J.* **2003**, *9*, 4991–4996. [[CrossRef](#)] [[PubMed](#)]
12. Woo, K.; Lee, H.J.; Ahn, J.P.; Park, Y.S. Sol-gel mediated synthesis of Fe<sub>2</sub>O<sub>3</sub> nanorods. *Adv. Mater.* **2003**, *15*, 1761–1764. [[CrossRef](#)]
13. Teng, X.; Yang, H. Effects of surfactants and synthetic conditions on the sizes and self-assembly of monodisperse iron oxide nanoparticles. *J. Mater. Chem.* **2004**, *14*, 774–779. [[CrossRef](#)]
14. Yu, A.C.C.; Mizuno, M.; Sasaki, Y.; Kondo, H.; Hiraga, K. Structural characteristics and magnetic properties of chemically synthesized CoPt nanoparticles. *Appl. Phys. Lett.* **2002**, *81*, 3768–3770. [[CrossRef](#)]
15. Fan, X.; Guan, J.; Wang, W.; Tong, G. Morphology evolution, magnetic and microwave absorption properties of nano/submicrometre iron particles obtained at different reduced temperatures. *J. Phys. D Appl. Phys.* **2009**, *42*, 075006. [[CrossRef](#)]
16. Zhou, M.; Zhang, X.; Wei, J.; Zhao, S.; Wang, L.; Feng, B. Morphology-controlled synthesis and novel microwave absorption properties of hollow urchinlike  $\alpha$ -MnO<sub>2</sub> nanostructures. *J. Phys. Chem. C* **2010**, *115*, 1398–1402. [[CrossRef](#)]
17. Gao, B.; Qiao, L.; Wang, J.; Liu, Q.; Li, F.; Feng, J.; Xue, D. Microwave absorption properties of the Ni nanowires composite. *J. Phys. D Appl. Phys.* **2008**, *41*, 235005. [[CrossRef](#)]
18. Xie, B.Q.; Qian, Y.; Zhang, S.; Fu, S.; Yu, W. A Hydrothermal Reduction Route to Single-Crystalline Hexagonal Cobalt Nanowires. *Eur. J. Inorg. Chem.* **2006**, *2006*, 2454–2459. [[CrossRef](#)]
19. Tong, G.; Hu, Q.; Wu, W.; Li, W.; Qian, H.; Liang, Y. Submicrometer-sized NiO octahedra: Facile one-pot solid synthesis, formation mechanism, and chemical conversion into Ni octahedra with excellent microwave-absorbing properties. *J. Mater. Chem.* **2012**, *22*, 17494–17504. [[CrossRef](#)]

20. Wang, W.; Wang, C.G.; Guo, Y. Fabrication and microwave characteristics of Fe<sub>3</sub>O<sub>4</sub>/C composites. *Adv. Mater. Res. Trans Tech Publ.* **2012**, *430*, 146–149. [[CrossRef](#)]
21. Hu, C.; Mou, Z.; Lu, G.; Chen, N.; Dong, Z.; Hu, M.; Qu, L. 3D graphene–Fe<sub>3</sub>O<sub>4</sub> nanocomposites with high-performance microwave absorption. *Phys. Chem. Chem. Phys.* **2013**, *15*, 13038–13043. [[CrossRef](#)] [[PubMed](#)]
22. Xu, H.L.; Bi, H.; Yang, R.B. Enhanced microwave absorption property of bowl-like Fe<sub>3</sub>O<sub>4</sub> hollow spheres/reduced graphene oxide composites. *J. Appl. Phys.* **2012**, *111*, 07A522. [[CrossRef](#)]
23. Singh, V.K.; Shukla, A.; Patra, M.K.; Saini, L.; Jani, R.K.; Vadera, S.R.; Kumar, N. Microwave absorbing properties of a thermally reduced graphene oxide/nitrile butadiene rubber composite. *Carbon* **2012**, *50*, 2202–2208. [[CrossRef](#)]
24. Gadelrab, K.R.; Chiesa, M.; Bonilla, F.A. Implications of the idea of effective tip shape on nanoindentation unloading curves: AFM measurements and FE simulation. *J. Mater. Res.* **2012**, *27*, 126–131. [[CrossRef](#)]
25. Chen, C.Y.; Pu, N.W.; Liu, Y.M.; Huang, S.Y.; Wu, C.H.; Ger, M.D.; Chou, Y.C. Remarkable microwave absorption performance of graphene at a very low loading ratio. *Compos. Part B Eng.* **2017**, *114*, 395–403. [[CrossRef](#)]
26. Cao, W.Q.; Wang, X.X.; Yuan, J.; Wang, W.Z.; Cao, M.S. Temperature dependent microwave absorption of ultrathin graphene composites. *J. Mater. Chem. C* **2015**, *3*, 10017–10022. [[CrossRef](#)]
27. He, J.Z.; Wang, X.X.; Zhang, Y.L.; Cao, M.S. Small magnetic nanoparticles decorating reduced graphene oxides to tune the electromagnetic attenuation capacity. *J. Mater. Chem. C* **2016**, *4*, 7130–7140. [[CrossRef](#)]
28. Chen, C.Y.; Pu, N.W.; Liu, Y.M.; Chen, L.H.; Wu, C.H.; Cheng, T.Y.; Grubb, P.M. Microwave absorption properties of holey graphene/silicone rubber composites. *Compos. Part B Eng.* **2018**, *135*, 119–128. [[CrossRef](#)]
29. Wang, C.; Han, X.; Xu, P.; Zhang, X.; Du, Y.; Hu, S.; Wang, X. The electromagnetic property of chemically reduced graphene oxide and its application as microwave absorbing material. *Appl. Phys. Lett.* **2011**, *98*, 072906. [[CrossRef](#)]
30. Hummers, W.S., Jr.; Offeman, R.E. Preparation of graphitic oxide. *J. Am. Chem. Soc.* **1958**, *80*, 1339. [[CrossRef](#)]
31. Mao, Z.; Wang, W.; Liu, Y.; Zhang, L.; Xu, H.; Zhong, Y. Infrared stealth property based on semiconductor (M)-to-metallic (R) phase transition characteristics of W-doped VO<sub>2</sub> thin films coated on cotton fabrics. *Thin Solid Films* **2014**, *558*, 208–214. [[CrossRef](#)]
32. Bi, A.; Zhu, J. Hydrothermal synthesis of W and Mo co-doped VO<sub>2</sub> (B) nanobelts. *J. Exp. Nanosci.* **2013**, *8*, 46–53. [[CrossRef](#)]
33. Bai, X.; Zhai, Y.; Zhang, Y. Green approach to prepare graphene-based composites with high microwave absorption capacity. *J. Phys. Chem. C* **2011**, *115*, 11673–11677. [[CrossRef](#)]
34. Quan, L.; Qin, F.X.; Estevez, D.; Wang, H.; Peng, H.X. Magnetic graphene for microwave absorbing application: Towards the lightest graphene-based absorber. *Carbon* **2017**, *125*, 630–639. [[CrossRef](#)]
35. Wang, Y.Q.; Cheng, R.M.; Wen, Z.; Zhao, L. Synthesis and Characterization of Single-Crystalline MnFe<sub>2</sub>O<sub>4</sub> Ferrite Nanocrystals and Their Possible Application in Water Treatment. *Eur. J. Inorg. Chem.* **2011**, *2011*, 2942–2947. [[CrossRef](#)]
36. Gao, Y.; Zhao, Y.; Fu, M.; Jiao, Q.; Li, H. Microemulsion-mediated solvothermal synthesis of hollow Co–Ni ferrite nanoparticle tubes and their magnetic properties. *Micro Nano Lett.* **2013**, *8*, 68–69. [[CrossRef](#)]
37. Zhang, Z.; Rondinone, A.J.; Ma, J.X.; Shen, J.; Dai, S. Morphologically templated growth of aligned spinel CoFe<sub>2</sub>O<sub>4</sub> nanorods. *Adv. Mater.* **2005**, *17*, 1415–1419. [[CrossRef](#)]
38. Zhang, X.F.; Guan, P.F.; Dong, X.L. Multidielectric polarizations in the core/shell Co/graphite nanoparticles. *Appl. Phys. Lett.* **2010**, *96*, 223111. [[CrossRef](#)]
39. Kim, S.S.; Kim, S.T.; Yoon, Y.C.; Lee, K.S. Magnetic, dielectric, and microwave absorbing properties of iron particles dispersed in rubber matrix in gigahertz frequencies. *J. Appl. Phys.* **2005**, *97*, 10F905. [[CrossRef](#)]
40. Che, R.; Peng, L.M.; Duan, X.F.; Chen, Q.; Liang, X.L. Microwave absorption enhancement and complex permittivity and permeability of Fe encapsulated within carbon nanotubes. *Adv. Mater.* **2004**, *16*, 401–405. [[CrossRef](#)]
41. Wang, W.; Zang, C.; Jiao, Q. Synthesis, structure and electromagnetic properties of Mn–Zn ferrite by sol–gel combustion technique. *J. Magn. Magn. Mater.* **2014**, *349*, 116–120. [[CrossRef](#)]
42. Ren, X.; Xu, G. Electromagnetic and microwave absorbing properties of NiCoZn-ferrites doped with La<sup>3+</sup>. *J. Magn. Magn. Mater.* **2014**, *354*, 44–48. [[CrossRef](#)]

43. Wang, C.; Han, X.; Zhang, X.; Hu, S.; Zhang, T.; Wang, J.; Xu, P. Controlled synthesis and morphology-dependent electromagnetic properties of hierarchical cobalt assemblies. *J. Phys. Chem. C* **2010**, *114*, 14826–14830. [[CrossRef](#)]
44. Li, H.; Huang, Y.; Sun, G.; Yan, X.; Yang, Y.; Wang, J.; Zhang, Y. Directed growth and microwave absorption property of crossed ZnO netlike micro-/nanostructures. *J. Phys. Chem. C* **2010**, *114*, 10088–10091. [[CrossRef](#)]
45. Luo, H.; Gong, R.; Wang, X.; Song, K.; Zhu, C.; Wang, L. Synthesis and excellent microwave absorption properties of reduced graphene oxide/FeNi<sub>3</sub>/Fe<sub>3</sub>O<sub>4</sub> composite. *New J. Chem.* **2016**, *40*, 6238–6243. [[CrossRef](#)]
46. Sun, G.; Dong, B.; Cao, M.; Wei, B.; Hu, C. Hierarchical dendrite-like magnetic materials of Fe<sub>3</sub>O<sub>4</sub>,  $\gamma$ -Fe<sub>2</sub>O<sub>3</sub>, and Fe with high performance of microwave absorption. *Chem. Mater.* **2011**, *23*, 1587–1593. [[CrossRef](#)]
47. Ufimtsev, P.Y.; Ling, R.T.; Scholler, J.D. Transformation of surface waves in homogeneous absorbing layers. *IEEE Trans. Antennas Propag.* **2000**, *48*, 214–222. [[CrossRef](#)]
48. Ling, R.T.; Scholler, J.D.; Ufimtsev, P.Y. The propagation and excitation of surface waves in an absorbing layer. *Prog. Electromagn. Res.* **1998**, *19*, 49–91. [[CrossRef](#)]
49. Li, Y.; Li, D.; Wang, X.; Nie, Y.; Gong, R. Influence of the electromagnetic parameters on the surface wave attenuation in thin absorbing layers. *AIP Adv.* **2018**, *8*, 056616. [[CrossRef](#)]



© 2018 by the authors. Licensee MDPI, Basel, Switzerland. This article is an open access article distributed under the terms and conditions of the Creative Commons Attribution (CC BY) license (<http://creativecommons.org/licenses/by/4.0/>).